Al-Azhar University Civil Engineering Research Magazine (CERM)
Vol. (40) No. (4) October, 2018

THE BEHAVIOR OF BOX GIRDERS UNDER DYNAMIC LOADS

Hussein Abbas[1], Emad Salem [2], and Ahmed Fawzi[3]

[1] Professor of Steel Structures at the Civil Engineering Department, Azhar University, Cairo.
[2]Associate Professor of Steel Structures at the Civil Engineering Department, Azhar University, Cairo.
[3] Teaching Assistant of Steel Structures at the Civil Engineering Department, Azhar University, Cairo.

ملخص البحث

لقد اصبحت الكبارى الصندوقية المركبة نظام انشائى شائع الاستخدام فى كبارى الطرق السريعة نتيجة لاعتبارات تتعلق بالاحمال الثقيلة والتكلفة والشكل الجمالى. هذا البحث يعرض الاستجابة الديناميكية للكبارى المركبة تحت تاثير احمال المركبات الثقيلة. وللوصول لهذا الهدف فان معاملات الصدم للكبارى المركبة تعطى اطروحة شاملة للسلوك الديناميكى العام ، لقد تم عمل نماذج ثلاثية الابعاد خلال هذه الدراسة ، الأول وكان نموذج تحقيق للتأكد من صلاحيته بمقارنة النتائج بتجارب معملية سابقة ، النتائج اعطت قيم قريبة ومتفقة مع القيم المتحصل عليها من الاختبارات المعملية ، أما النموذج الثانى كان لدراسة الحمل الديناميكى بتعريض الكوبرى ذو بحر 40 متر لاحمال سيارات بسرعات مختلفة ، الشاحنة المستخدمة كانت طبقا لمواصفات الكود الاوروبى جزء احمال السيارات EN 1991-2-2003. وقد اوضحت النتائج ان معامل التضخيم الديناميكى للاجهاد والازاحات يزداد مع سرعة السيارة، علاوة على ان القيم الذروة للعجلة تزداد ايضا مع زيادة السرعة.

ABSTRACT

Due to the heavy loads and economic and aesthetic considerations, multi-cell composite box girder bridges became a very popular statically system in highway bridges. This paper presents the dynamic response of composite box girder under heavy vehicular loads. To reach this goal, the study of impact factors for the composite box girder bridge gives a comprehensive approach for the global dynamic behavior. 3-D finite element models was conducted through the study. The first, was to verify the results obtained by a previous experimental work, and to validate the accuracy of computer program. The results showed a good agreement with experimental study. The second, studied the dynamic behavior by exposing multi-steel concrete box girder bridge of span 40 m to vehicular load with different speed. The truck loading configuration according to Eurocode, EN: 1991-2:2003[2] part, Traffic loads on bridges. The results indicated that DAF_s for stress and displacement increase with the increase of vehicles speed, in addition to the peak acceleration also increase with the increase of vehicles speed.

1. INTRODUCTION

Many searches have been conducted to study the effect of static and dynamic analysis on composite steel box girder bridges. However, the dynamic effect is more challengeable than the static analysis due to the complexity of analysis and the significant deterioration of the box cross section. Box girder bridges distort primarily due to torsional moments caused by eccentrically applied loads. Torsional moments can be divided into equivalent force that can rotate the girder about its longitudinal axis and distort the cross-sectional shape. These torsional moments are resisted internally by a combination of St. Venant[1] torsion and warping torsion however the St. Venant[1] torsional stiffness is dominant over the warping torsional stiffness in a box section that result from a closed cross section. Torsional warping in the boxes are usually relatively small and are not considered in the design of box girders. (Kollbrunner and Basler 1969) [3]

Composite multi-cell box girder bridges were constructed to endure the heavy loads induced by the moving vehicles. However, the dynamic effect of moving load may cause large deformations and sometimes, the structure may collapse. The source of disturbance can be Transient, wind, or seismic loads on abridge that cause dynamic deflections due to bridge oscillations and may cause discomfort for pedestrians and motorists, particularly when the fundamental frequency is mainly torsional. The fundamental frequency of a bridge is the main characteristic in investigating the effects due to dynamic loads imposed on the structure. High dynamic response is to be expected only if bridge resonant frequencies coincide with the fundamental spectrum of the truck wheel load. So, dynamic amplification factor (*DAF*) is presented to magnify the maximum straining action exerted by a moving vehicle to study the effect of dynamic loads.

Chopra (1995)[4] evaluate the dynamic amplification for single degree of freedom system with harmonic excitation as follow,

$$DAF = \frac{1}{\sqrt{[1-(\omega/\omega_n)^2]^2+[2\zeta(\omega/\omega_n)]^2}} \quad (1\text{-}1)$$

Many resea tors. This paper will mention briefly the previous work includes the dynamic load came from moving vehicle and trains. (Galdos and Schelling,1990)[5] studied the dynamic response of horizontally curved multi-spine box girder bridges of a different spans. Results for the impact factors formed the basis for those currently used by AASHTO Guide Specification for horizontally curved highway bridges for curved multi-spine box girder bridges. (Huang, et al, 1997) [6] developed a procedure to investigate the dynamic response of thin-walled curved box girder bridges due to truck loading and to get their basic impact characteristics, the results indicated that most impact factors of torsion and distortion much larger than those of vertical bending response.

(Senthilvasan, et al, 2002)[7] studied the dynamic response of twin box girder bridges under the passage of a heavy vehicle at different speeds. Strains and deflections were recorded. It was noticed a good agreement for the values of dynamic factors with the analytical bridge-vehicle interaction model and the values those obtained by design codes. (Gong and Cheung, 2008)[8] evaluated the dynamic response for box girder bridges by using finite element method. The bridge-vehicle interaction is affected by many factors such as vehicle speed, road roughness, damping of the bridge and vehicle and the dynamic characteristics of the bridge. Parametric study has been carried out to investigate those factors that influence the bridge-vehicle interaction.

(Amanat and Hossain, 2010)[9] presents an investigation of the dynamic responses of the cantilever slab of a concrete box girder bridge subjected to moving traffic loads. The dynamic deformation responses of the bridge are evaluated for different vehicle speeds. Dynamic amplification factors (DAF) are evaluated by comparing the tip deflection of the cantilever slab found from dynamic analysis to the same obtained from static analysis, and the effects of vehicle speed and span length on DAF were found to be significant.

(Kim et al , 2014)[10] studied the dynamic responses of a high speed railroad steel composite bridge experimentally. Measured responses show that the vertical displacements of tested bridges all satisfy requirements for passenger comfort, but

vertical acceleration responses were also found to be very close to the limit value for traffic safety. It was found that most of the excessive acceleration responses occurred when the passing speed of the train is close to the critical speed which causes resonance. Also, the dynamic amplification factor varies with the change of the damping ratio.
(Rezaie et al 2015)[11] examined the bridge under the passage of six heavy vehicles at different speeds so as to determine its static and dynamic responses. The bridge vibrates at a fundamental frequency of 2.6 Hz intensively and the first mode of vibration is torsional instead of flexural. (CHEUNG et al, 1999) **[12]** analyzed the vibration of a multi-span non-uniform bridge subjected to a moving vehicle. Passive tuned mass damper (PTMDs) was used to decay motion of train-induced vibration on the bridge. The results show that only .5% (PTMDs), can reduce the vertical acceleration of the bridge by 40%.

2. METHODOLEGY OF MOVING LOAD ON SIMPLE BEAM

To study the dynamic response for simple beam, Consider a concentrated load P_0 travel along a beam of span L with constant speed V_0 . At the any instant t the load P_0 is at a distance $a=V_0t$ from the left support as shown in **Fig. 1**, flexure rigidity of the beam EI.

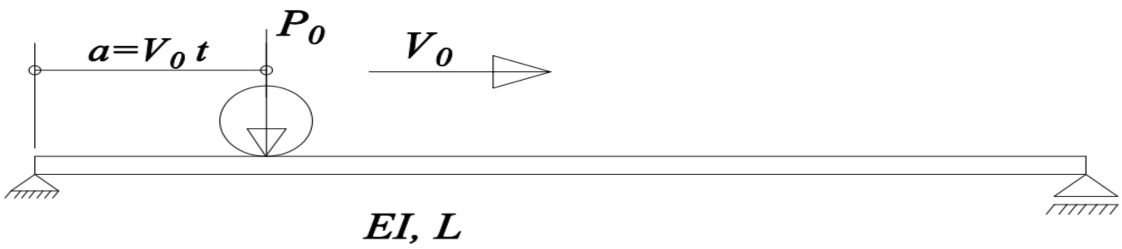

Fig .1. Simple beam excited by moving load

The load distribution at this instant can be written by the harmonic series (Volterra and Zachmanoglou, 1965)[13] as:

$$P(\mathrm{x,t}) = (2P0/\mathrm{L})[\sin(\frac{\pi V\,0t}{L})\sin(\frac{\pi x}{L}) + \sin(\frac{2\pi V\,0t}{L})\sin(\frac{2\pi x}{L}) + \sin(\frac{3\pi V\,0t}{L})\sin(\frac{3\pi x}{L}) + \ldots\ldots\ldots] \quad (1)$$

Let $\acute{\omega} = \dfrac{\pi V\,0}{L}$ so Equation (3.28) will be,

$$P(\mathrm{x,t}) = (2P0/\mathrm{L})[\sin(\acute{\omega}t)\sin(\frac{\pi x}{L}) + \sin(2\acute{\omega}t)\sin(\frac{2\pi x}{L}) + \sin(3\acute{\omega}t)\sin(\frac{3\pi x}{L}) + \ldots\ldots\ldots] \quad (2)$$

Thus, the response of the beam can be obtained as:

$$U(x,t) = (\frac{2p_0L^3}{\pi^4 EI})\{\frac{\sin(\frac{\pi x}{L})}{1-(\frac{\bar{\omega}}{\omega n})^2}[\sin(\bar{\omega}t) - (\frac{\omega}{\omega n})\sin(\omega nt)] + \frac{\sin(\frac{2\pi x}{L})}{2^4-(\frac{2\bar{\omega}}{\omega n})^2}[\sin(2\bar{\omega}t) - (\frac{\bar{\omega}}{2\omega n})\sin(2^2\omega nt) + \frac{\sin(\frac{3\pi x}{L})}{3^4-(\frac{3\bar{\omega}}{\omega n})^2}[\sin(3\bar{\omega}t) - (\frac{\bar{\omega}}{3\omega n})\sin(3^3\omega nt) + \ldots..\} \quad (3)$$

This series give the dynamic deflection at any point through simple beam subjected to moving load and can be further used to simulate the moving vehicle through the bridges.

3. EXAMPLE

Timoshenko simple beam is modelled with span L=40 m, E= 29.43GPa, Shear Modulus G=12.26GPa, weight per unit length $\acute{m}$ = 36056 Kg/m, cross section area $A=7.94$ m^2 , moment of inertia I=8.72 m^4, damping ratio $\zeta=0.03$, and shear coefficient $\acute{k}$ = 0.41, (Younesian, 2008)[14] The fundamental frequency of simple beam can be obtained by (Chopra, 2002)[4] as:

$$\omega_n = \frac{\pi^2}{L^2}\sqrt{\frac{EI}{m}} \qquad (4)$$

This value is very close the values obtained by (Younesian, 2008)[14] and the value extracted from ABAQUS as shown in Tab. (1).

Tab. 1 Values of natural frequency obtained by three methods

Flexure Beam Theory	ABAQUS	Younesian
16.45 rad/s	18.8 rad/s	16.09 rad/s

This beam was reused by F. Javid (2011)[15] with damping ratio $\zeta=0.01$. The velocity chosen in this study was 20 m/s and the load magnitude was 200 kN. The critical velocity obtained by (Volterra,1965)[13] as:

$$V_0 = \omega_n L/\pi \qquad (5)$$

The beam was simulated by ABAQUS Standard to extract the natural frequency as shown in **Fig. 2 a, b.** The next step, ABAQUS Explicit with Vdload Subroutine was used to model the moving load through the beam, Rayleigh Damping is necessity in the analysis of dynamic integration method to obtain quantitatively accurate results. Rayleigh Damping factors can be obtained by using Eq.(6), (7) for the first and the second mode natural frequency. The result indicate a good agreement obtained by F. Javid, as shown in **Fig. 3**.

$$\alpha = 2\,\zeta\,\omega_i\,\omega_j\,/\,\omega_i+\omega_j \qquad (6)$$

$$\beta = 2\zeta/\,\omega_i+\omega_j \qquad (7)$$

α = 0.121813, β = 0.000375

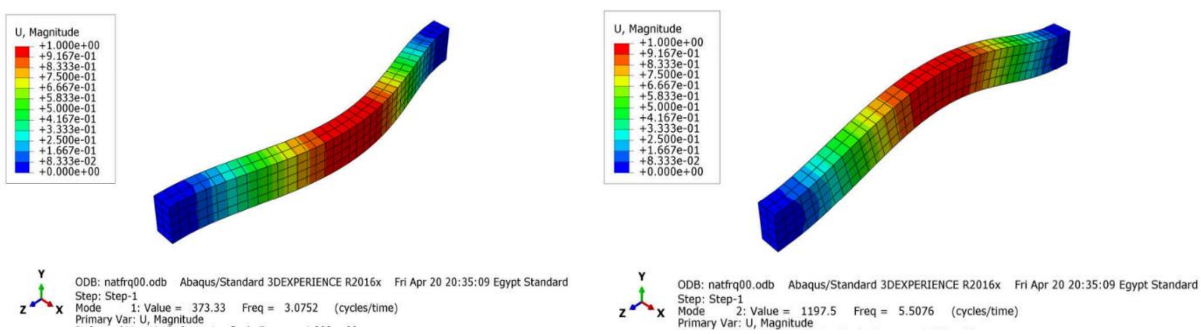

(a) **(b)**

Fig .2 a, b First and second natural mode of the beam

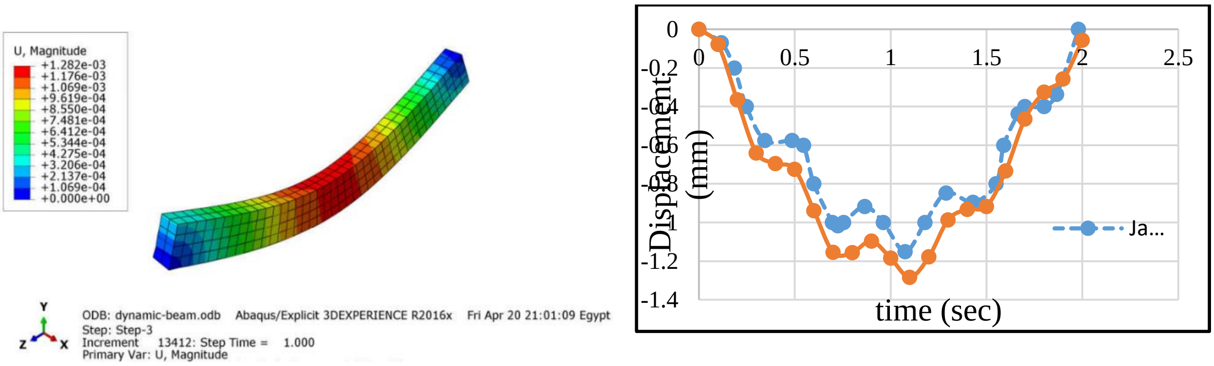

Fig. 3. Deflection of the beam by ABAQUS Explicit and comparison with Javid results.

4. EXPERIMENTAL VERIFICATION

Experimental testing of a small-scale twin steel box-girder bridge specimen has been incorporated in this paper to investigate the static behavior in linear and nonlinear range. The experimental work was done by (Pham, 2016)[16]. Each box-girder was designed to have two internal diaphragms at the supports and two cross-frames at every one-third length of the main span and one internal cross frame 600mm away from the cantilever end. The specimen cantilever length was 3048 mm. All detailed information of the specimen as shown in **Fig. 4, 5.**

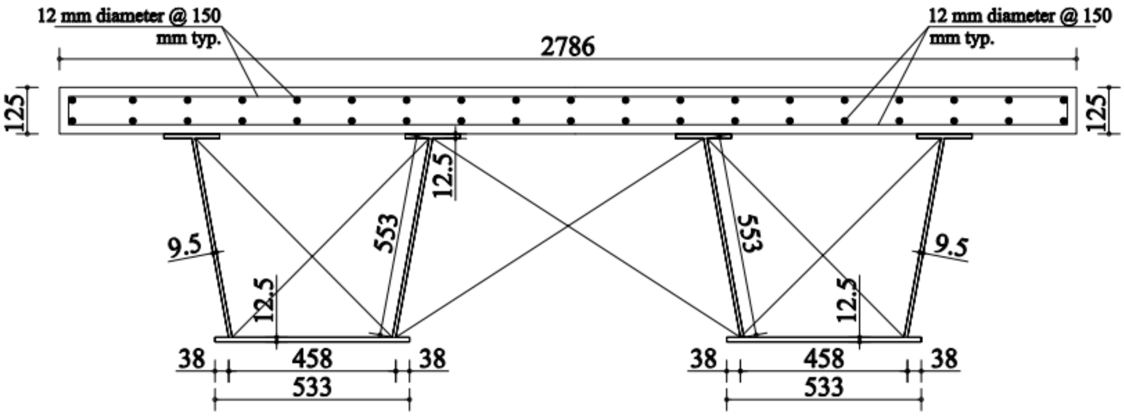

Fig Error! No text of specified style in document.. **Cross-section of the tested specimen**

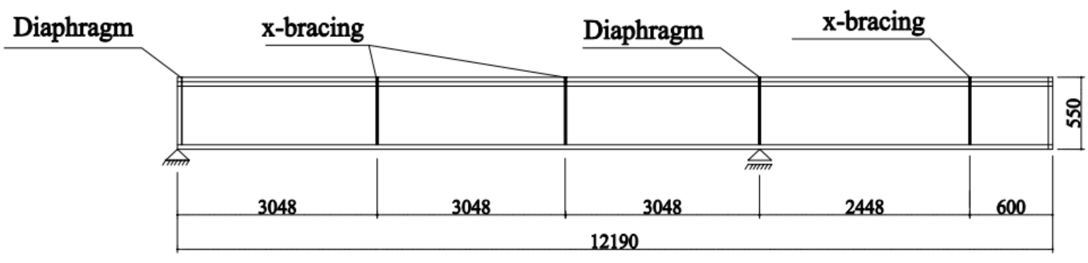

Fig .5. Cross-bracing and diaphragm positions

Steel plates are grade 50 steel and were assumed to have yield strength of 344 MPa and compressive strength of concrete was 31 MPa after with 28-day for design purposes. The reinforcements are grade 60 steel and were assumed to have yield strength of 413 MPa. Loading system used for this experiment, two actuators, a loading beam (stiff I-beam) and steel reinforced elastomeric bearing pads. One actuator has 3558 kN capacity and the other one has a 2001 kN capacity. Under this loading setup, one or two-point loading scenarios can be executed. **Fig .6** shows the complete specimen that was clearly prepared to be tested.

Fig .6 Specimen with complete loading setup. (Pham, 2016)[16]

5. Elastic Test

This test was carried out on the undamaged specimen to evaluate the elastic behavior of scaled box girder. In the elastic test, the load was applied to the specimen through 50 x 25 x 900 mm^3 loading pad(s). The applied loads were selected to be 222 kN over each box in order to ensure the responses of the specimen to be in a linear range under undamaged condition. The maximum displacements for east and west girder were 8.05, 8.23 respectively. **Fig.7** illustrates the elastic loading condition.

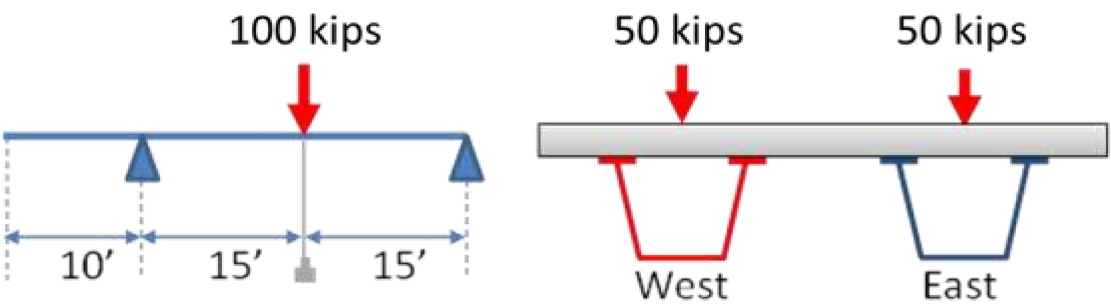

Fig .7 Schematic description of elastic test (Pham, 2016)[16]

6. Ultimate Test

The ultimate load test was carried to capture the nonlinear behavior of box girder bridge as well as maximum capacity at the moment of bridge failure. The bridge specimen was tested under a full-web fracture damage condition. The load was applied through a displacement-controlled hydraulic ram, over the damaged girder at the mid-span location. The specimen reached its maximum capacity at 687 kN with 63 mm. of displacement, the discerption of ultimate test illustrated in **Fig .8**.

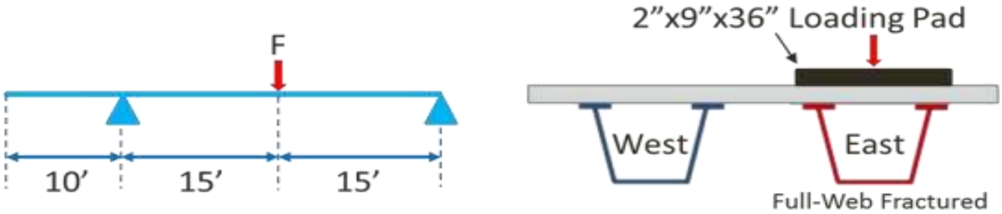

Fig. 8. Schematic description of ultimate test (Pham, 2016)[16]

7. Finite Element Modelling

ABAQUS, a finite element modeling software simulation. Material nonlinearities were taken into account when modeling both steel and concrete behavior. The steel materials were assumed to have multi-linear isotropic hardening responses. The concrete was also modeled as a multi-linear isotropic hardening material. The contact areas between the steel girder or the deck and pads were also taken into consideration in modeling.

The steel plate girder was modeled using 4-node shell element, S4R with six degrees of freedom at each node. The stiffeners and the interior diaphragms were also modeled by S4R elements. However, the interior and exterior cross-frames and lateral bracings were modeled by using A 2-node linear beam B31 in with six degree of freedom at each node. The concrete deck was also modeled using S4R with six degrees of freedom at each node. The perfect plastic behavior was assumed when the stress exceeded yield stress, Von Mises plasticity was incorporated.

The steel plates, steel bracing members, and steel reinforcement were A709 Grade 50 steel and young's modulus, E= 250750 (MPa) while the steel reinforcement bars were A706 Grade 60 reinforcement and young's modulus, , E= 300900 (MPa) . The stress-strain curves of the steel plates and rebar shown in **Fig. 9, and 10** are approximations of typical stress-strain curves of A709 Grade 50 steel and A706 Grade 60 steel reinforcements under uniaxial tension load.

Class II concrete mix with 28-day strength of 31 MPa. The average of all concrete compressive strength cylinder tests was 54 N/mm^2, and this is the value used in respective simulated finite element models. The average tensile strength of concrete was found to be 3.75 N/mm^2. Concrete compressive behavior was constructed using **Eq. (8)** (Pham, 2016)[50] as suggested by Hognestad (1951). With the ultimate strain (ε_0=0.003), modulus of elasticity, 33000 N/mm^2. The stress-strain curve of concrete under uniaxial compressive force is graphically illustrated in **Fig. 11**.

$$f_c = f_c' \left(2 * \varepsilon / \varepsilon_0 - (\varepsilon / \varepsilon_0)^2\right) \tag{8}$$

where,

fc = concrete compressive stress at given strain (N/mm^2)
fc' = concrete compressive strength (N/mm^2)
ε_0 = ultimate strain (mm/mm)
ε = strain (mm/mm)

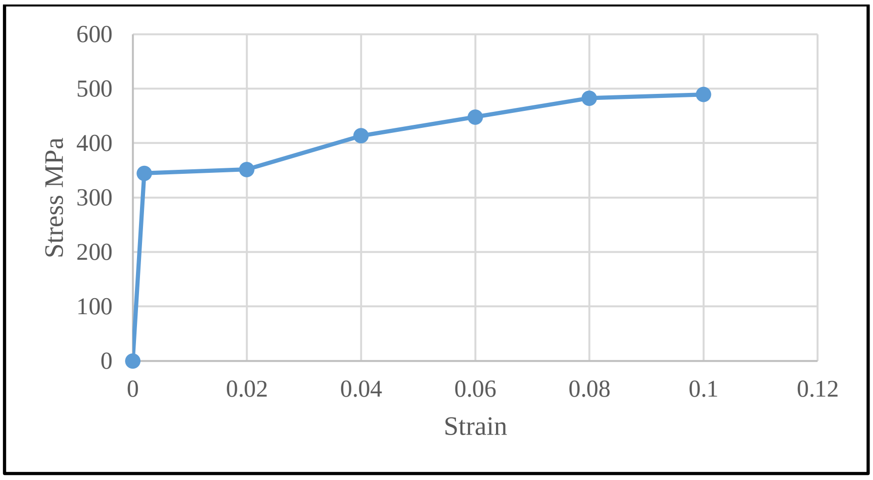

Fig. 9. Stress-strain behavior of steel plates (Pham, 2016)[50]

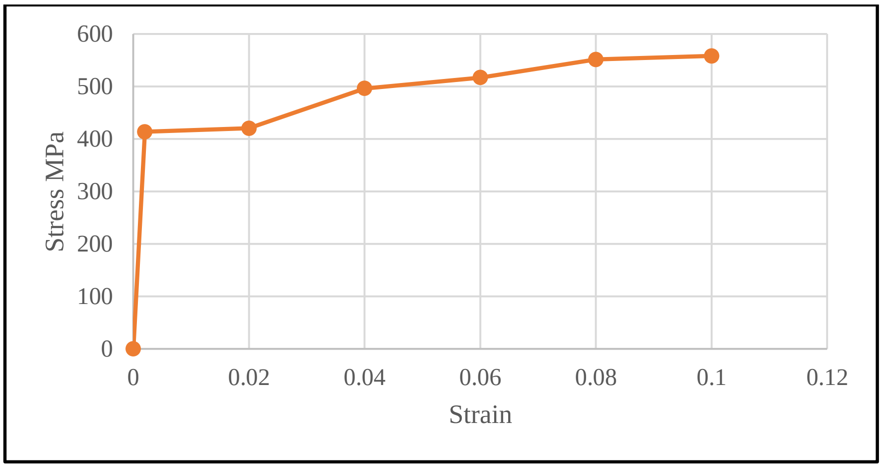

Fig. 10. Stress-Strain Behavior of Steel Rebar (Pham, 2016)[50]

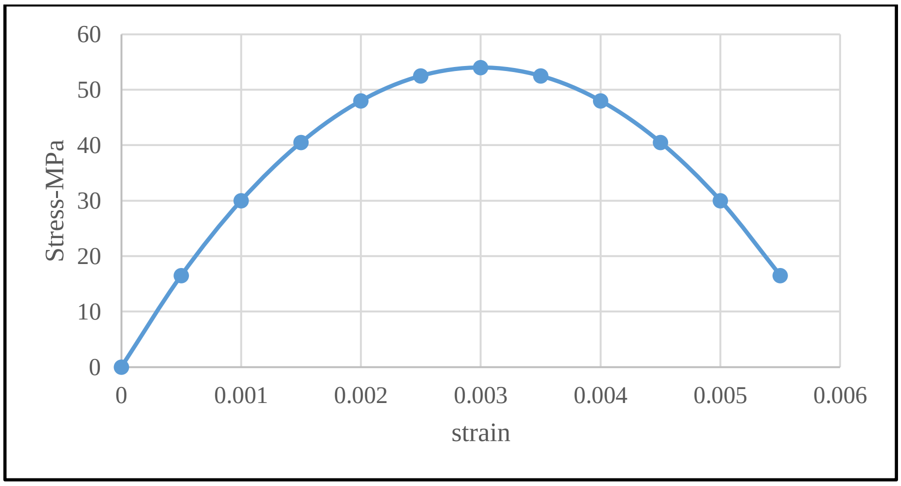

Fig. 11. Stress-strain curve for concrete

Defining plasticity data in ABAQUS require to determine true stress and plastic strain. True strain is defined as:

$$6 = 6_{nom} \, (1+\varepsilon_{nom}) \qquad (9)$$

The relation between true strain and nominal strain is defined as:

$$\varepsilon_{true} = ln(1+\varepsilon_{nom}) \qquad (10)$$

Thought, the relation between plastic strain and true strain can be demonstrated as:

$$\varepsilon_{plastic} = \varepsilon_{true} - 6/E \qquad (11)$$

The steel plate girder-concrete slab interface was modeled by interface elements available within the ABAQUS element library. Using penalty coefficient formulation with friction coefficient .3. Hard contact used to define contact in normal direction. In addition, the two surfaces cannot penetrate each other. The shear forces across the steel plate girder and concrete slab are transferred by the mechanical action of headed stud shear connectors. The headed stud diameter was 19 mm and a height 100 mm and were placed at 200 mm longitudinally welded in the top flange. The load-slip characteristic of headed stud has been conducted from pushout test analysis. Pushout was performed to investigate the nonlinear behavior of 9 shear studs welded in steel flange and embedded in concrete, the results indicated in **Fig. 12, and 13**

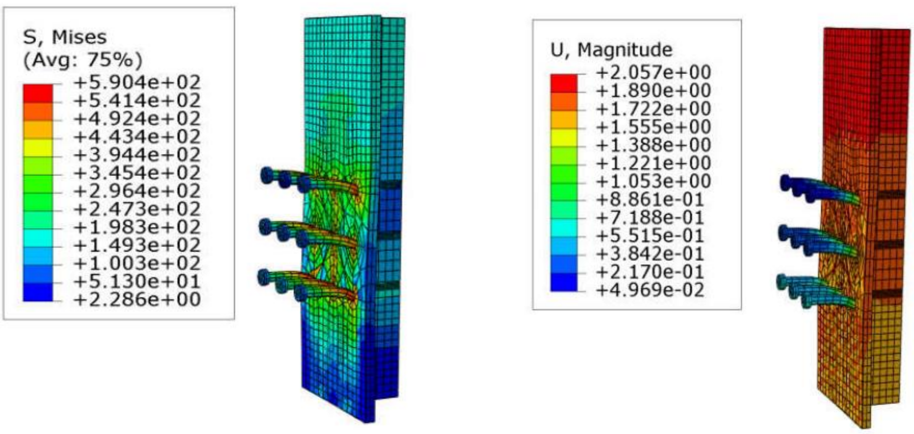

Fig. 12. Pushout test results model for 9 shear stud

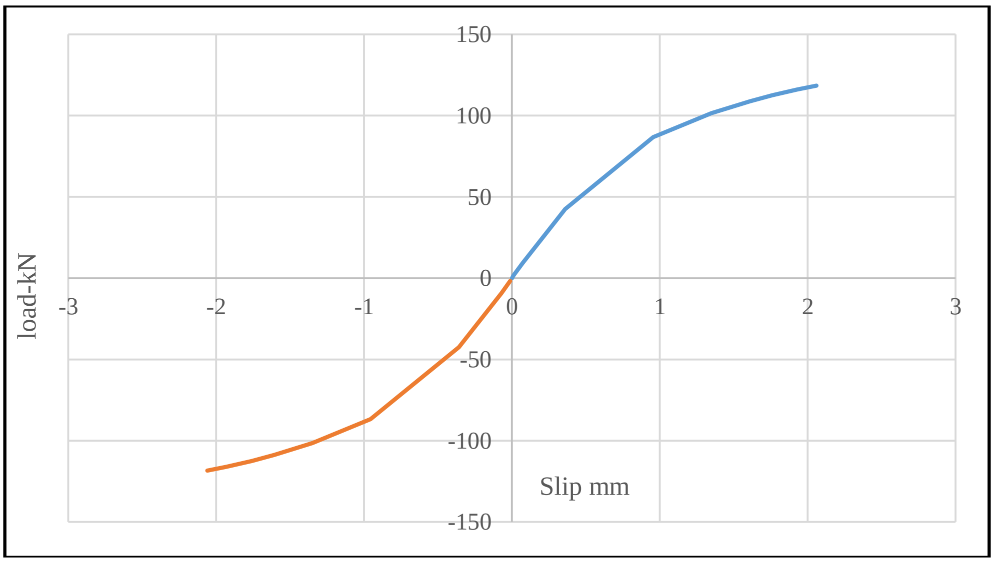

Fig .13. Load-Slip curve for one stud

The finite element analysis results are compared to the experimental data on selected tests. **Fig. 14, and 15** indicates a 3-D finite element model for the two cases of loading .The comparison will be for the displacement at the mid-span section. The vertical displacements at the center of the bottom flange of both girders at the mid-span section are compared with those obtained from experimental tests, **Fig. 16, and 17**. The results shows a good agreement with those obtained from the experimental results, as shown in **Fig. 18, and 19.**

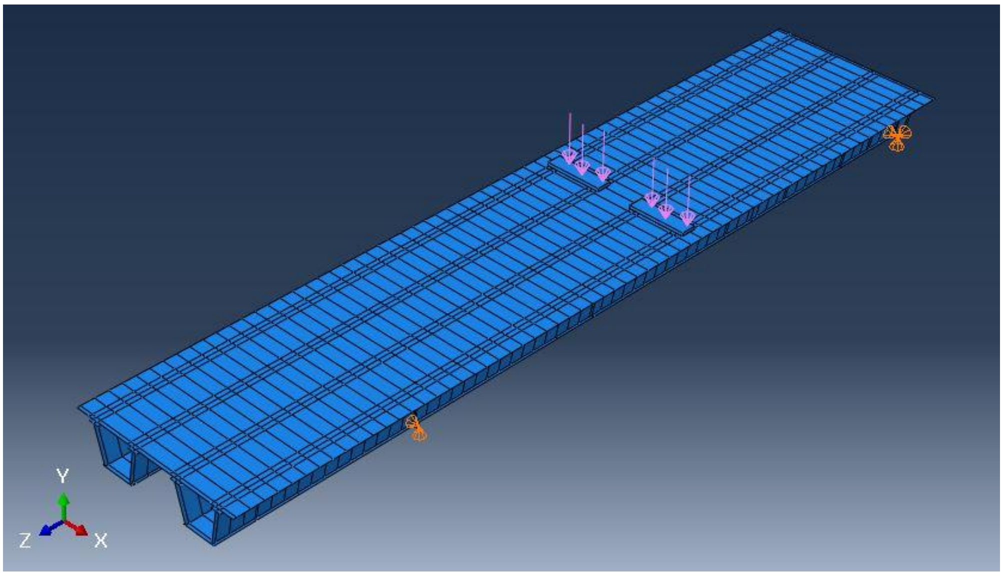

Fig .14. 3-D finite element model for elastic test

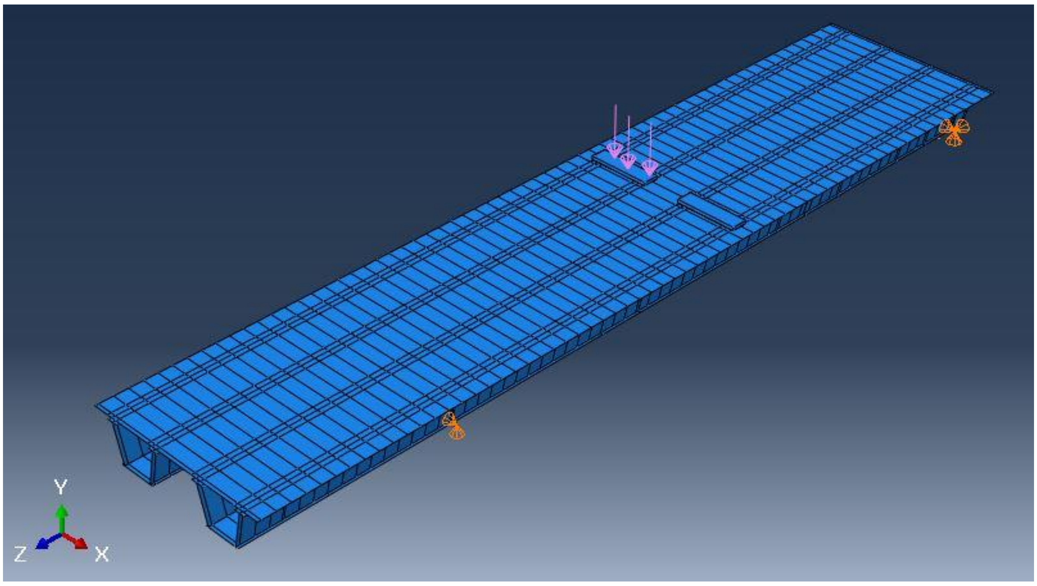

Fig .15. 3-D finite element model for Ultimate test

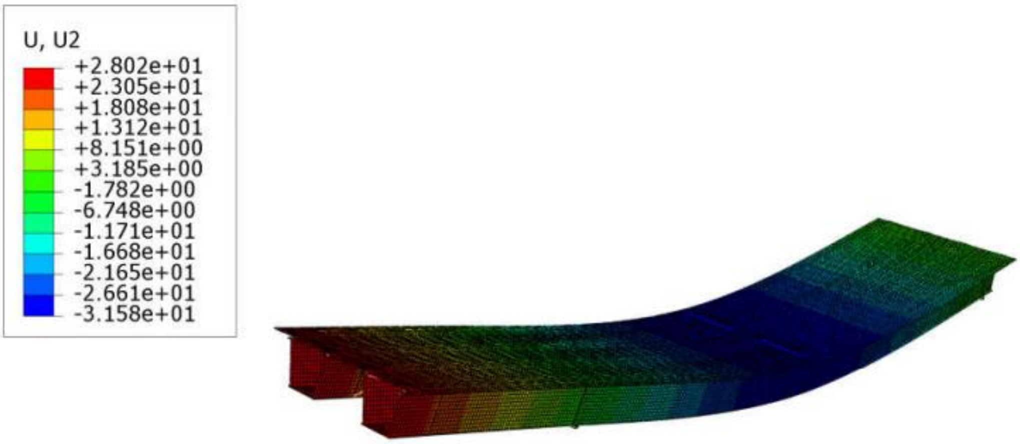

Fig. 16. Vertical displacement for elastic test

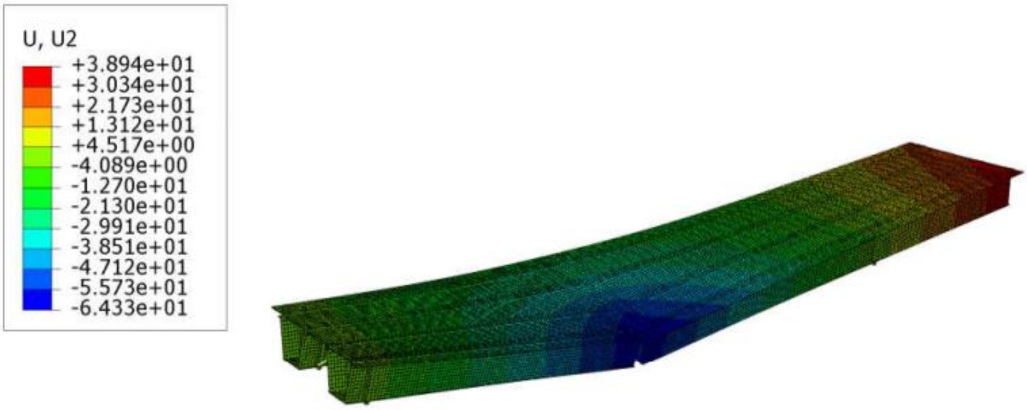

Fig. 17. Vertical displacement for Ultimate test

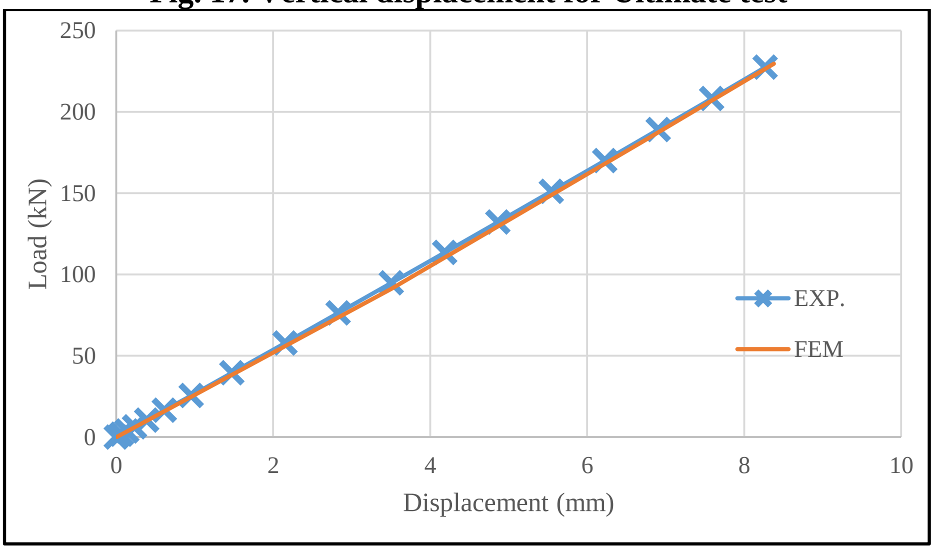

Fig. 18. Comparison between F.E results and experimental for load-displacement at the bottom of intact girder flange

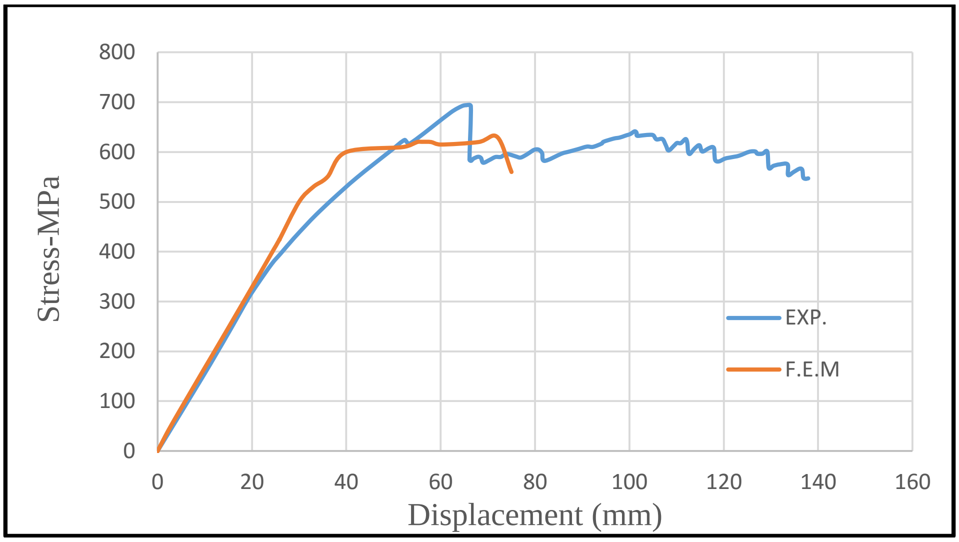

Fig. 19. Comparison between F.E results and experimental for load-displacement at the midpoint of the deck at mid span

8. FINITE ELEMENT MODEL FOR STRAIGHT BOX GIRDER BRIDGE

A full-scale 3D finite element model for composite box girder bridge was built by commercial finite element program ABAQUS. Three main parts should be simulated to figure out the dynamic response of the box bridge. First, The static procedure that will be simulated by using ABAQUS Standard. Second, extracting of fundamental frequency of the bridge. Free vibration analysis and the frequency perturbation procedure will be also simulated by using ABAQUS Standard. The last, the dynamic analysis for the box girder bridge subjected to different speed and the comparison with the static load. The static procedure will be simulated by using ABAQUS Explicit. The study include symmetric and non-symmetric loading conditions. The loading truck was according to Eurocode BS EN 1992-2[2] which used in evaluating the fatigue of bridges.

Parametric studies were performed on single span straight box girder bridge. The objectives of the finite element model were to examine the influence of the truck speed on the structural response. Establish a data base for the impact factors, for maximum stresses and deflection for the design purposes. Investigation the effect of loading mechanism on the dynamic amplification factor for the maximum stress and deflection in addition the peak value of acceleration for mid-span bottom flange point.

9. Bridge Description

Full scale composite box girder bridge with span of 40m and practical range of span-to-depth ratio was nearly 22. The deck of the bridge was concrete of thickness 22.5 *cm* connected with two cell steel box girder by shear stud connector. **Fig. 20** indicates the geometry of the bridge cross section.

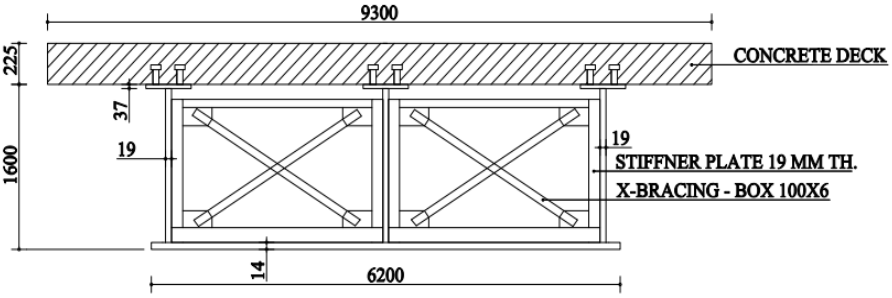

Fig. 20. Geometry of composite box girder

Exterior diaphragms were provided outside the box girders at each support. The end diaphragm thicknesses were taken to be the same as those of the webs. The depth of the diaphragms was taken the same as the depth of the steel box. Intermediate cross bracings with upper top chords were placed at a spacing of 6.6 m to resist torsion. **Fig. 21** shows positions of the internal cross bracing and the exterior diaphragms.

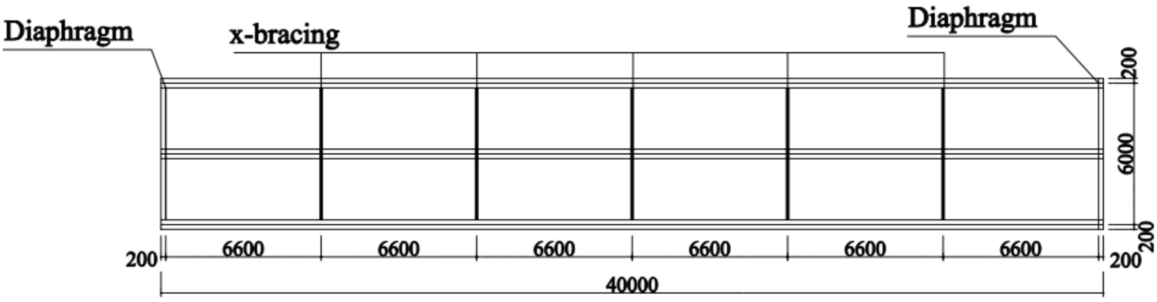

Fig. 21. Positions of x-bracings and diaphragms

The steel plate girder, the stiffeners and the exterior diaphragms was modeled using 4-node shell element, S4R with six degrees of freedom at each node. However, the interior and cross-frames and top chord bracings were modeled by using a 2-node linear beam B31H in with six degree of freedom at each node. The concrete deck was also modeled using C3D8R, an 8-node linear brick, reduced integration with eight degrees of freedom at each node. Steel rebars were modelled by using a T3D2, a 2-node linear 3-D truss element. The moduli of elasticity of concrete and steel were taken as 27 and 200 GPa, respectively. Steel girders had a specified minimum yielding stress of 350 MPa. Compressive strength for concrete was 54 MPa. Possion's ratio was taken as 0.2 for concrete and 0.3 for steel. The densities for concrete and steel was 2400 Kg/m^3, 7800 Kg/m^3 respectively. The material is considered an isotropic, elastic and homogeneous for both steel and concrete. Boundary constraints with hinged support at the end of the bridge. The second was, the roller support at other end. The contact between upper steel flange and the bridge deck can be modelled tie constraint option to ensure full interaction between the concrete deck slab and the steel cells.

The loading was represented by the fatigue truck that used in Eurocode BS EN 1992-2: 2003, Table 4.7 and 4.8, with a total weight 390 kN. Fatigue truck was used for simulating the live load acing on the bridge. The idealization of the truck and the axle position and the magnitude of wheel loadings **Fig. 22 a, b**

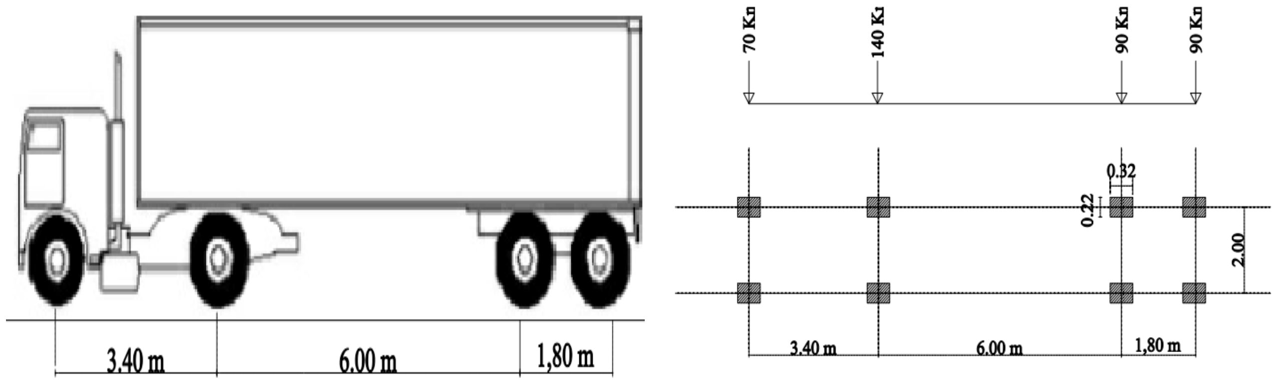

a **b**

Fig. 22 a, and b. Fatigue load vehicle according to BS EN 1992-2: 2003

The truck were positioned at different cases of loading. Where, the truck take the form of symmetric and non-symmetric loading position as shown in **Fig. 23 a, and b.**

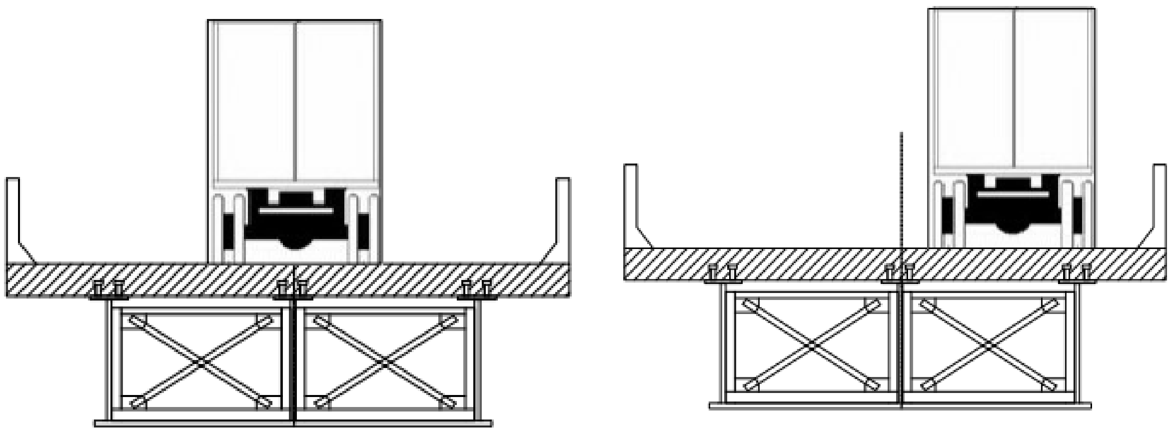

a. symmetric loading **b- non symmetric loading**

Fig. 23 a, and b Mechanism of symmetric and non-symmetric loading

In order to model moving truck running statically with a constant velocity through ABAQUS Standard, Dload subroutine was written through FORTRAN and linked with ABAQUS by the compatibility between FORTRAN compiler and ABAQUS Standard. The tire was simulated as a moving plate with dimensions 0.32x0.22 m^2 that is similar to the dimensions of tire presented by BS EN 1992-2: 2003. the speed was taken for the static moving load, 40 m/sec^2. Time history analysis was performed to evaluate the maximum Von Mises stresses and maximum deflection for the point located at mid-span for bottom flange. **Fig. 24, and 25** illustrate the results of stress and deflection for truck moving with constant speed 40 m/sec^2 for symmetric and non-symmetric loading mechanisms. The results indicate that changing load position had a slight difference of stress and displacement.

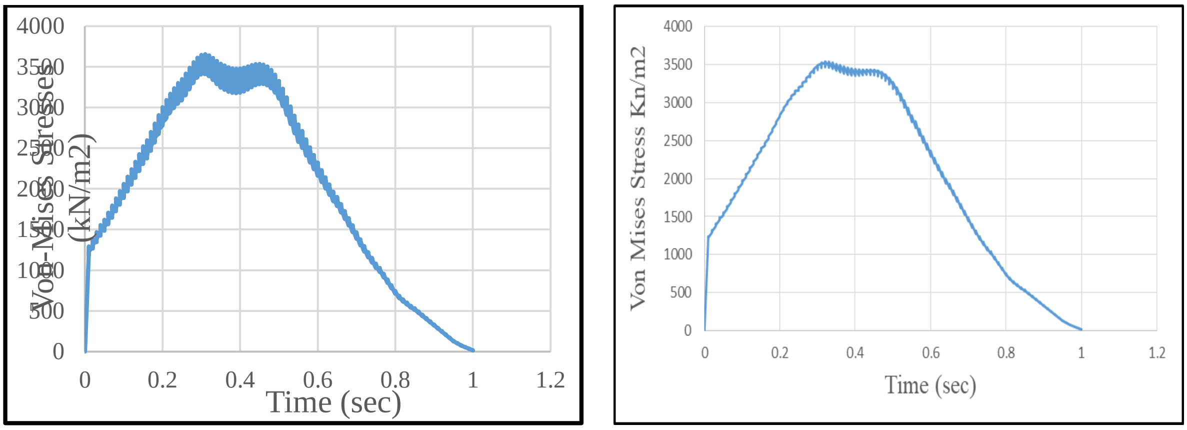

a. symmetric loading b. non-symmetric loading

Fig. 24 Static Von Mises Stresses -Time history of girder bottom flange at mid-span v=144 (Km/h)

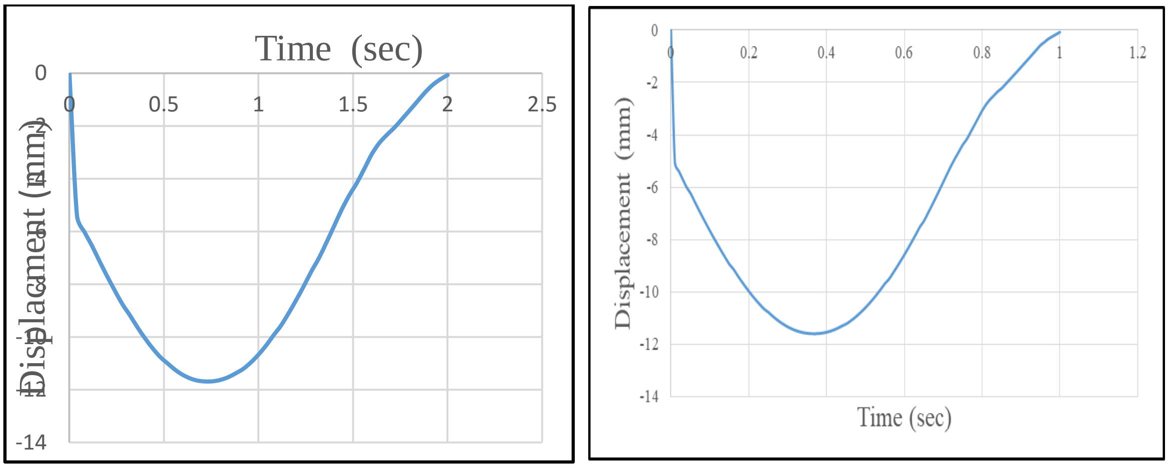

a. symmetric loading b. non-symmetric loading

Fig. 25 a, and b Static Displacement-Time history of girder bottom flange at mid-span v=144 (Km/h).

10. Natural Frequency Extraction

Free vibration linear dynamic analysis was performed to extract the natural frequency of the composite girder bridge. **Fig. 26 a, and b** indicate the first and second mode of deformation. The results of ABAQUS are very close to the result obtained by using flexure beam theory equation, (Chopra, 2002)[4] as shown at **Tab. 2**

Tab. 2 Comparison between the natural frequency obtained by ABAQUS and Flexure beam theory

Flexure beam theory	ABAQUS
10.658 rad/s	10.47 rad/s

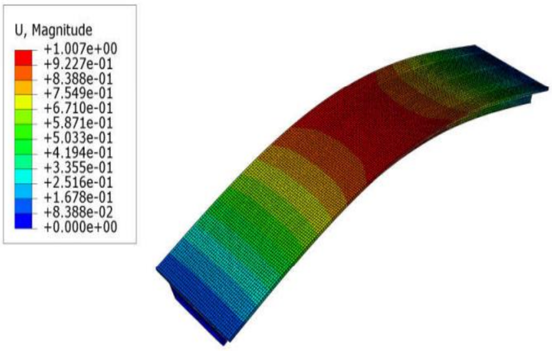

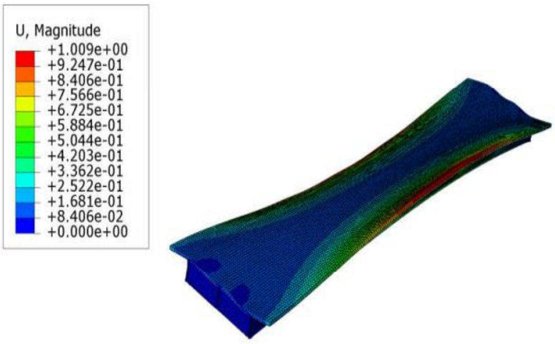

a. Mode 1 – Frequency 1.668 Hz b. Mode 2 – Frequency 4.605 Hz

Fig. 26 a, and b First and second fundamental frequency of the simulated bridge

11. Dynamic analysis

The forced-vibration analysis was carried out to study the effects of truck speed on the stress, displacement, and the peak acceleration at the bridge bottom flange. To obtain accurate values and more fast solution, dynamic explicit integration method was used. Explicit schemes obtain values for dynamic quantities at t+Δt based entirely on available values at time t. Material densities must be included at the model with consistent units for ABAQUS. The study includes the vehicle motion with various speeds, 36, 72, 108, and 144 Km/h. In order to simulate the moving truck over the bridge, Vdload user subroutine was written in FORTRAN to define the moving wheel loads as a function of position, time, and velocity. 8 Vdload subroutine were written for the four speeds in both symmetric and non-symmetric loading conditions. Each subroutine can be customized for the specific truck weight and speed. The wheel loads were applied as a uniformly distributed pressure over the contact area. Figure 5.10 a, b indicate the moving tire plate in both symmetric and non-symmetric loading mechanisms.

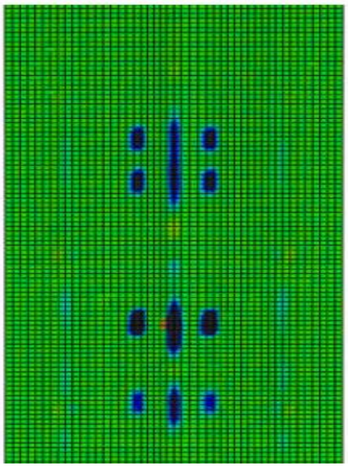

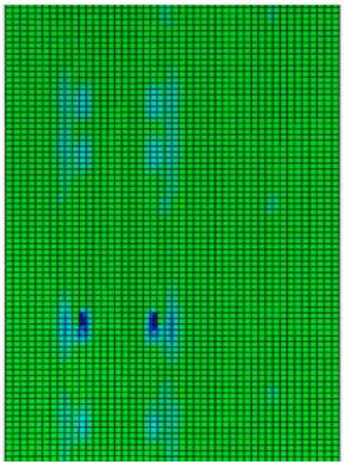

a. symmetric loading mechanisms b. non-symmetric loading mechanisms.

Fig. 26 a, and b Figure1.1 a, b. Idealization of truck position in ABAQUS

The results include the comparison between the static and dynamic responses for the displacement and stress at both cases of loading. The study was conducted by moving the truck with the specified speeds as shown in **Fig. 27 to 38**. The results indicate that the velocity affect significantly on the impact factors and the peak accelerations.

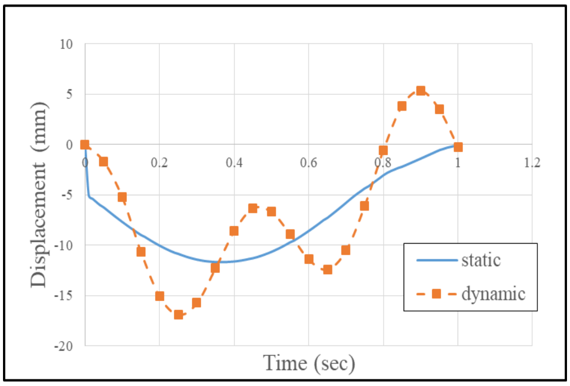

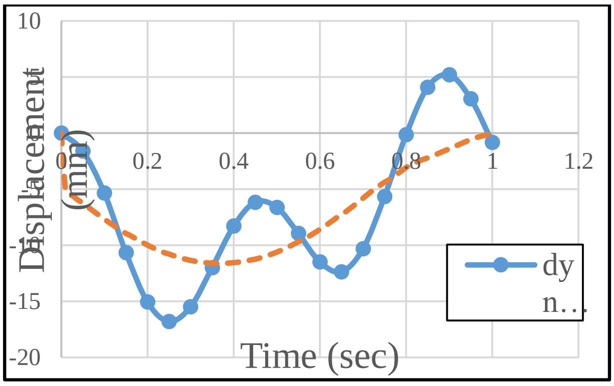

a. symmetric loading b. non-symmetric loading mechanisms.

Fig. 27. Displacement-Time history of girder bottom flange at mid-span (v=144 Km/h)

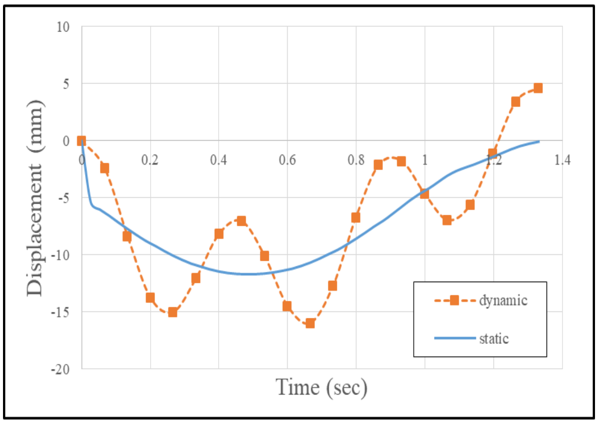

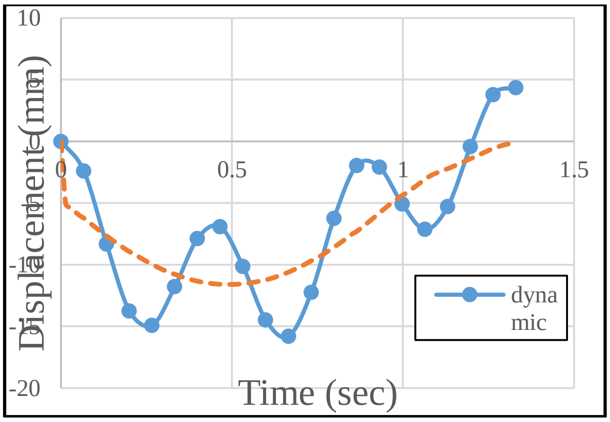

a. symmetric loading b. non-symmetric loading mechanisms.

Fig. 28. Displacement-Time history of girder bottom flange at mid-span (v=108 Km/h)

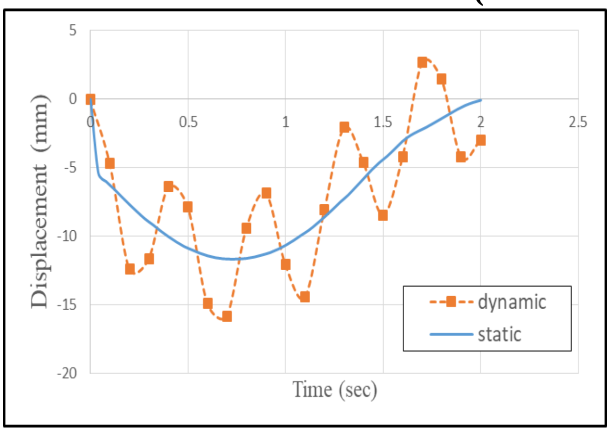

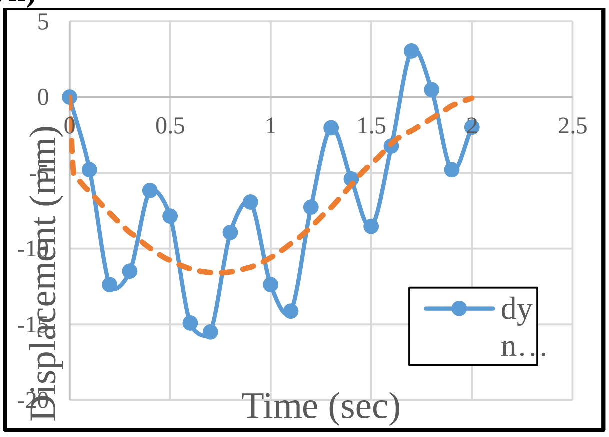

a. symmetric loading b. non-symmetric loading mechanisms.

Fig. 29. Displacement-Time history of girder bottom flange at mid-span (v=72 Km/h)

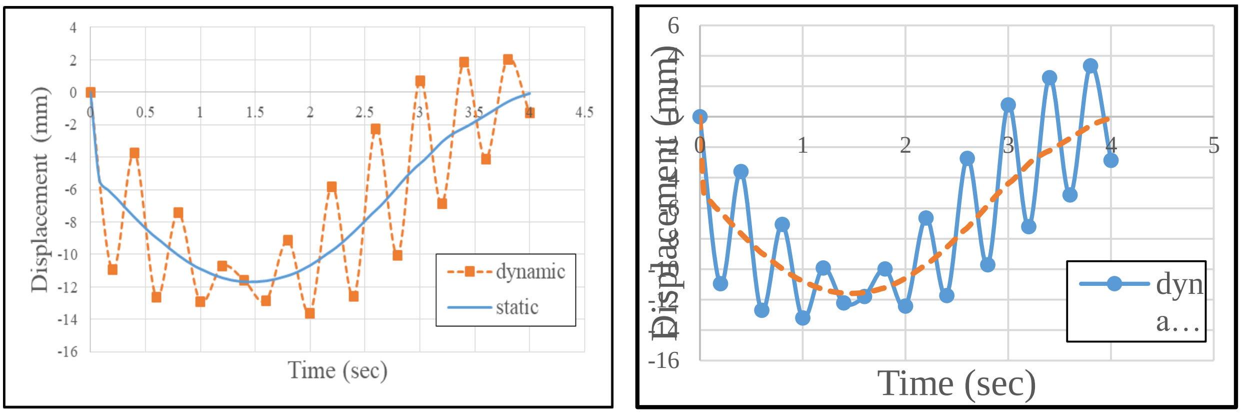

a. symmetric loading b. non-symmetric loading mechanisms.

Fig. 30. Displacement-Time history of girder bottom flange at mid-span (v=36 Km/h)

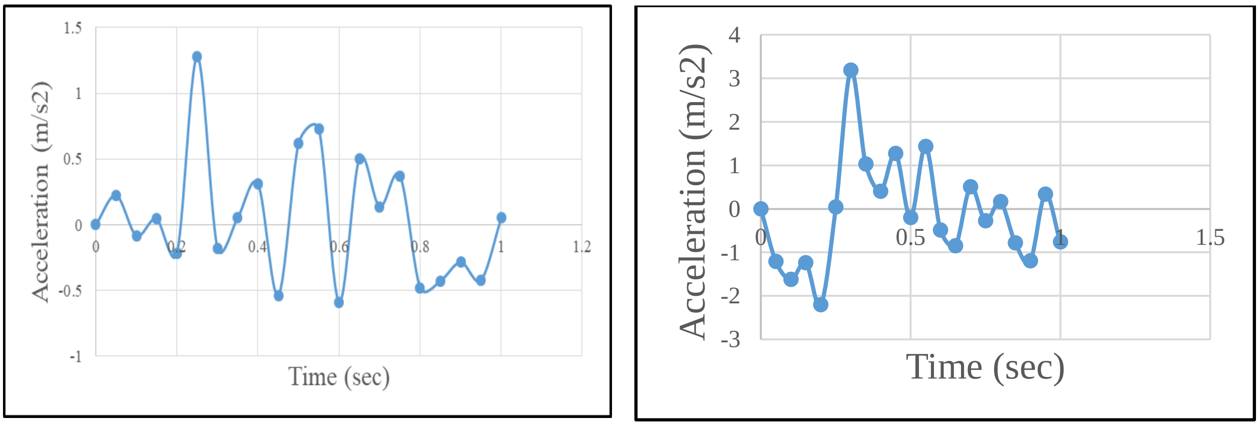

a. Symmetric loading b. non-symmetric loading mechanisms

Fig. 31. Acceleration-Time history of girder bottom flange at mid-span (v=144 Km/h)

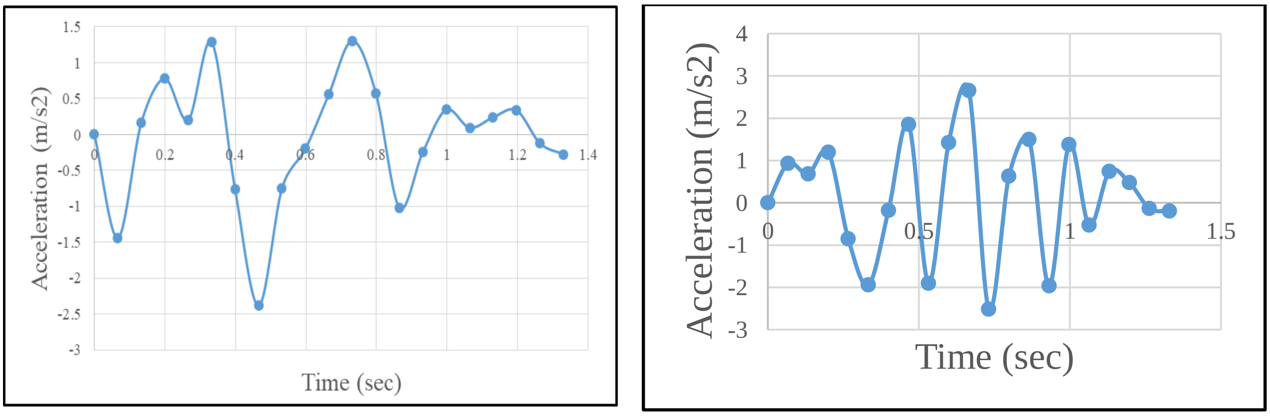

a. Symmetric loading b. non-symmetric loading mechanisms

Fig. 32. Acceleration-Time history of girder bottom flange at mid-span (v=108 Km/h)

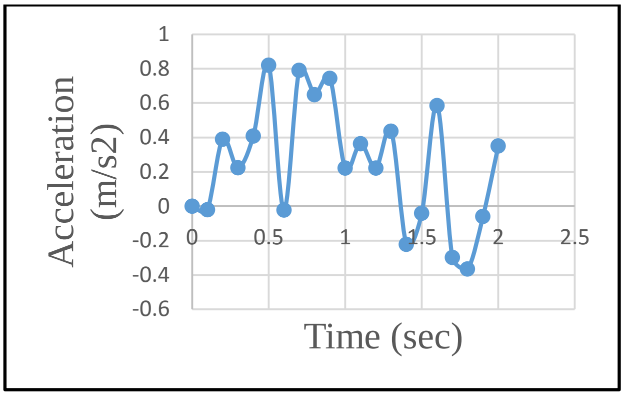

a. Symmetric loading

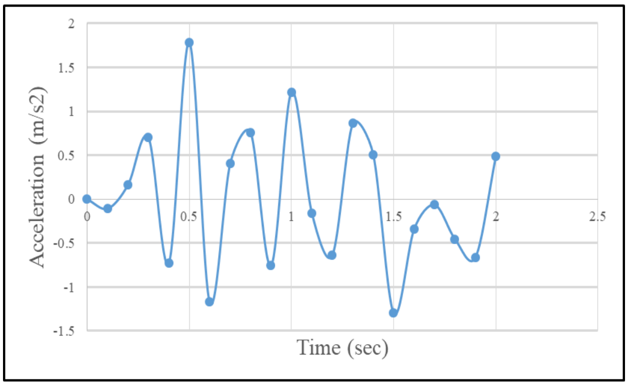

b. non-symmetric loading mechanisms

Fig. 33. Acceleration-Time history of girder bottom flange at mid-span (v=72 Km/h)

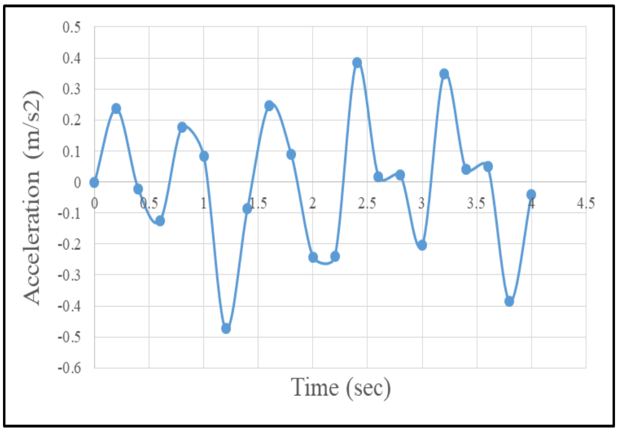

a. Symmetric loading

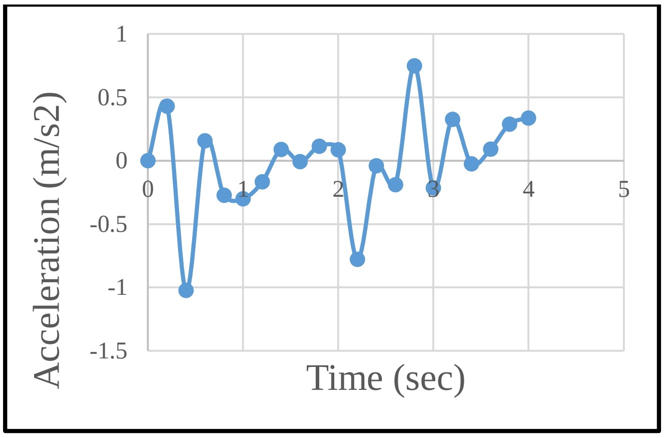

b. non-symmetric loading mechanisms

Fig. 34. Acceleration-Time history of girder bottom flange at mid-span (v=36 Km/h)

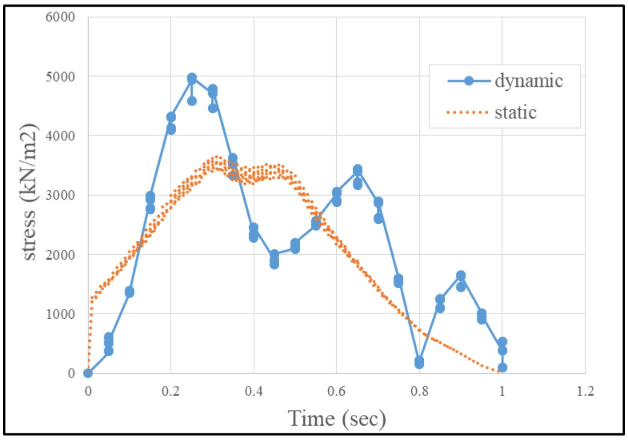

a. Symmetric loading

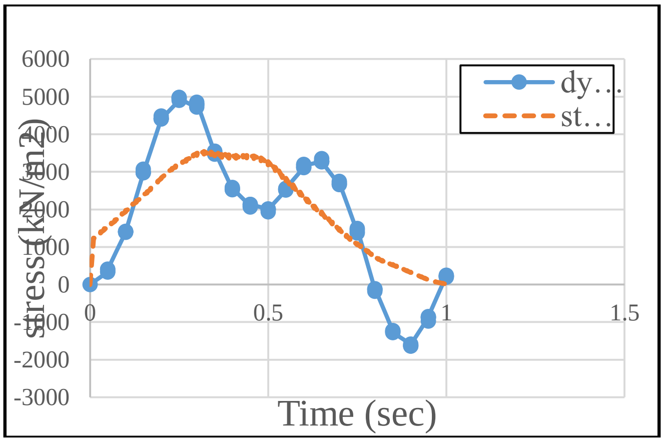

b. non-symmetric loading mechanisms

Fig. 35. Stress-Time history of girder bottom flange at mid-span (v=144 Km/h)

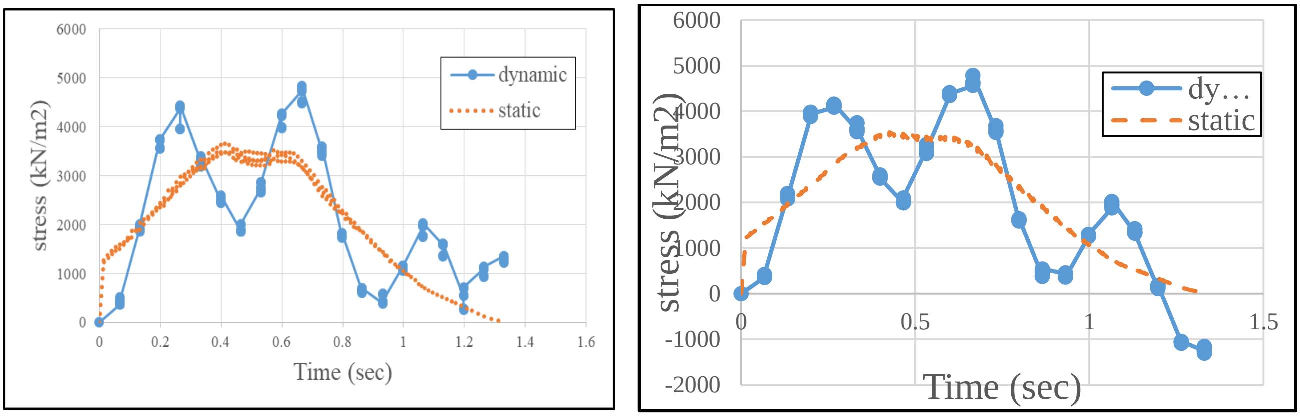

a. Symmetric loading b. non-symmetric loading mechanisms

Fig. 36. Stress-Time history of girder bottom flange at mid-span (v=108 Km/h)

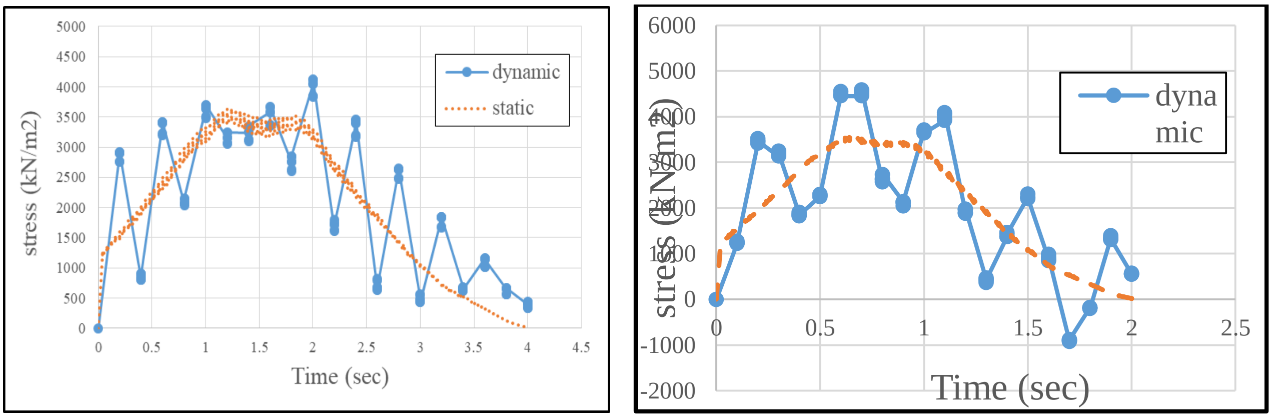

a. Symmetric loading b. non-symmetric loading mechanisms

Fig. 37. Stress-Time history of girder bottom flange at mid-span (v=72 Km/h)

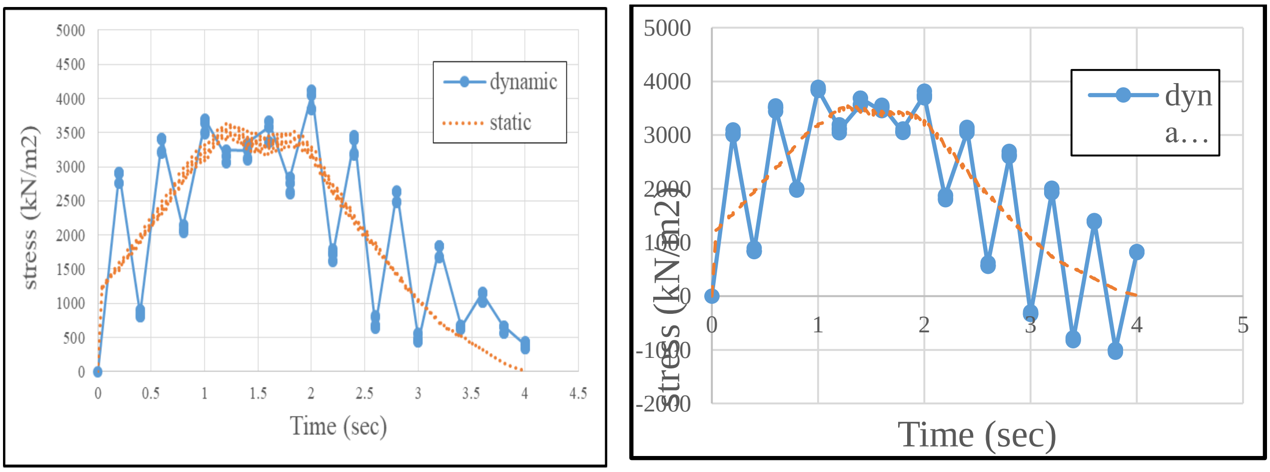

Fig. 38. Stress-Time history of girder bottom flange at mid-span (v=36 Km/h)

12. Dynamic Impact Factor

The effect of truck speed on impact factors is examined under symmetric and non-symmetric loading conditions, while the truck speed is selected within the maximum allowable safe speed. **Tab. 3** shows the effect of truck speed on the Stress, and deflection, for both cases. It can be clearly observed that the truck speed has a significant influence on impact factors. The impact factors increase significantly with increase in the truck speed for symmetric and non-symmetric loading mechanisms.

Tab. 3 Values of DAFs for Displacement and Stress at different speeds

Symmetric loading				
Speed (Km/h)		Static	Dynamic	DAF
144	Displacement (mm)	11.68	16.9	1.44
	Stress (kN/m^2)	3650	5012	1.37
108	Displacement (mm)	11.68	15.9	1.36
	Stress (kN/m^2)	3650	4852	1.33
72	Displacement (mm)	11.68	15.85	1.35
	Stress (kN /m^2)	3650	4677	1.28
36	Displacement (mm)	11.68	13.6	1.16
	Stress (kN /m^2)	3650	4175	1.14
Non-symmetric loading				
144	Displacement (mm)	11.59	16.8	1.45
	Stress (kN /m^2)	3527	4977	1.41
108	Displacement (mm)	11.59	15.72	1.36
	Stress (kN /m^2)	3527	4785	1.35
72	Displacement (mm)	11.59	15.5	1.33
	Stress (kN /m^2)	3527	4550	1.29
36	Displacement (mm)	11.59	12.4	1.06
	Stress (kN /m^2)	3527	3888	1.10

13. Effect of Vehicle Speed on peak acceleration

The maximum peak accelerations at various vehicle speeds, 36, 72, 108 and 144 km/h, were considered in the analysis. It can be observed that the accelerations are higher, generally, for non-symmetrical loading. In addition the speed increase with higher speeds. The peak acceleration occurred at a vehicle speed of 144 km/h. However, for symmetric loading, increasing the vehicle speed above 72 km/h, the peak acceleration increased. However, for vehicle speed 144km/h, the peak acceleration was lower than those obtained for vehicle speed of 108 km/h. the peak value occurred at vehicle speed of 108 Km/h as shown in **Fig. 39, and 40.**

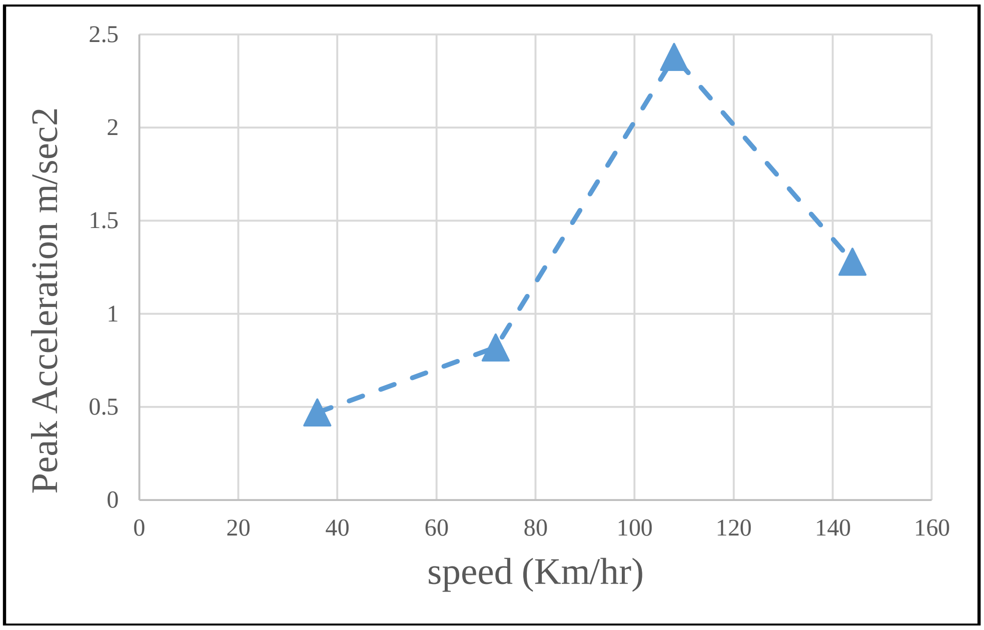

Fig. 39 Relation between the Peak Acceleration and Vehicle speed for symmetric loading mechanism

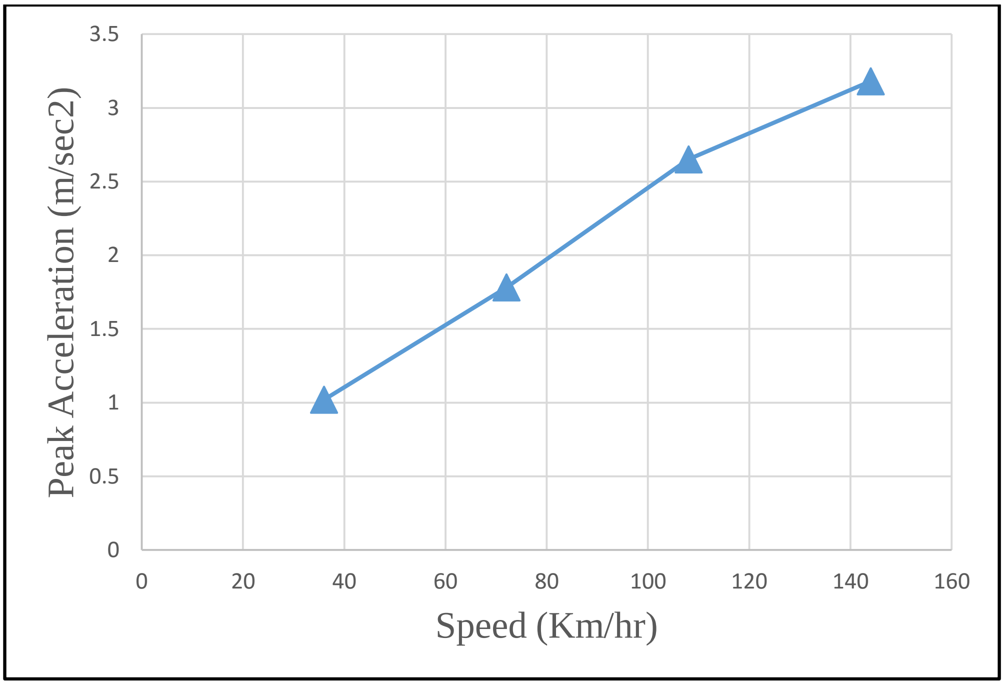

Fig. 40 Relation between the Peak Acceleration and Vehicle speed for non-symmetric loading mechanism

14. Conclusion

1. The fundamental frequency is the main characteristic aspect when the study of dynamic analysis.
2. Dynamic explicit integration method is more suitable method to simulate such complex structures of long span and linear and nonlinear analysis in addition to consuming the time and the cost of analysis.
3. Artificial damping has a small effect for suppression the vibration when comparing the obtained results with or without damping.
4. The DAF_s increase with the increase of truck speed.
5. The truck position did not effect on the DAF_s for displacement. However for stress the results was slightly different.
6. The peak acceleration increase with higher speeds for non-symmetric loading conditions and was bigger than the values obtained by the symmetric loading conditions.

REFERENCES

1. St. Venant[1] Castel A, Vidal T, Françis R. "Effective Tension Active Cross-Section of Reinforced Concrete Beams After Cracking" ;Engineering Structures, Vol. 39 No. 285, 2006, pp.115-126.
2. 1992-2, E., *Eurocode 3: Design of Steel Structures - Part: vehicular loads* 2003.
3. Helwig T, Yura J, Herman R, Williamson E, Li D. 4. Title and Subtitle Design Guidelines For Steel Trapezoidal Box Girder Systems. 2007;7(22)Akmaluddin, "Effect of Tensile Reinforcement Ratio on the Effective Moment of Inertia of Reinforced Lightweight Concrete Beams for Short Term Deflection Calculation" ITB J Eng Sci, Vol. 43 N. 3, 2011, pp.209-226.
4. Chopra anil k. *Dynamic of Structures*. 1st ed.; 1995.
5. Methodology for Impact Factor of Horizontally Curved Box Bridges By N. H. Galdos, ~ Associate Member, ASCE, D. R. Schelling, 2 Member, ASCE, and M. A. Sahin 3. 1993;119(6):1917-1934.Hong-Song Hu, Jian-Guo Nie, Yu-HangWang. "Effective Stiffness of Rectangular Concrete Filled Steel Tubular Members". Journal of Constructional Steel Research, Vol. 116, 2016, pp.233-246.
6. Huang D, Wang T-L, Shahawy M. Vibration of horizontally curved box girder bridges due to vehicles. *Comput Struct*. 1998;68(5):513-528. doi:10.1016/S0045-7949(98)00065-0.
7. Senthilvasan J, Thambiratnam DP, Brameld GH. Dynamic response of a curved bridge under moving truck load. *Eng Struct*. 2002;24(10):1283-1293. doi:10.1016/S0141-0296(02)00059-7.
8. Gong L, Cheung M. Computer simulation of dynamic interactions between vehicle and long span box girder bridges. *Tsinghua Sci Technol*. 2008;13(October):71-77. http://www.sciencedirect.com/science/article/pii/S1007021408701299
9. Hossain KA, Amanat KM. Effect of span length on the dynamic amplification factor in the deck of concrete box girder bridges. *J Civ Eng*. 2011;39(1):59-75.
10. Kim S, Kim H, Lee J. Dynamic responses of a steel composite bridge subjected to a moving high speed train load in comparison with a PSC box girder bridge. *WIT Trans Built Environ*. 2014;137:127-138. doi:10.2495/HPSM140121.
11. Rezaie F, Ahmadi G, Farnam SM. Load Test and Model Calibration of a Horizontally Curved Steel Box- Girder Bridge. *Civ Eng Infrastructures J*.

2015;48(2):305-322.

12. Wei-zhen L, Chang-ping C, Yi-qi M, Chang-zhao Q. Dynamic Analysis of Couple d Vehicle-Bri d ge System with Uniformly Variable Spee d. 2016;5(3):129-134. doi:10.1515/nleng-2016-0007.
13. Enrico Volterra ECZ. *Dynamics of Vibrations*.; 1965.
14. Younesian D, Kargarnovin MH, Esmailzadeh E. Optimal passive vibration control of Timoshenko beams with arbitrary boundary conditions traversed by moving loads. *Proc Inst Mech Eng Part K J Multi-body Dyn*. 2008;222(2):179-188. doi:10.1243/14644193JMBD121.
15. F. Javid. Vibration Suppression of Straight and Curved Beams Traversed by Moving Loads. – University of Ontario. Institute of Technology-2011.
16. Pham H V. Evaluation of Redundancy of Twin Steel Box-Girder Bridges. 2016. doi:10.25148/etd.FIDC001242.